Received: 13 May 2019 | Revised: 9 December 2019 | Accepted: 31 December 2019

DOI: 10.1096/fj.201901202RR

RESEARCH ARTICLE

THE FASEB JOURNAL

Inhibition of Ca^{2+} channel surface expression by mutant bestrophin-1 in RPE cells

Magdalena Cordes[1] | **Piotr Bucichowski**[1] | **Ahmad S. Alfaar**[1] | **Stephen H. Tsang**[3,4] | **Seba Almedawar**[2] | **Nadine Reichhart**[1] | **Olaf Strauß**[1]

[1]Experimental Ophthalmology, Department of Ophthalmology, Charité – Universitätsmedizin Berlin, a corporate member of Freie Universität, Humboldt-University, the Berlin Institute of Health, Berlin, Germany

[2]Center for Molecular and Cellular Bioengineering (CMCB), Center for Regenerative Therapies, Dresden (CRTD), Technische Universität Dresden, Dresden, Germany

[3]Jonas Children's Vision Care, and Bernard & Shirlee Brown Glaucoma Laboratory, Department of Ophthalmology, Columbia Stem Cell Initiative, Departments of Ophthalmology Pathology & Cell Biology, Institute of Human Nutrition, College of Physicians and Surgeons, Columbia University, New York, NY, USA

[4]Edward S. Harkness Eye Institute, New York-Presbyterian Hospital, New York, NY, USA

Correspondence
Olaf Strauß and Nadine Reichhart, Experimental Ophthalmology, Department of Ophthalmology, Charité – Universitätsmedizin, Campus Virchow Clinic, Augustenburger Platz 1, Berlin 13353, Germany.
Email: olaf.strauss@charite.de (O. S.) and Nadine.reichhart@charite.de (N. R.)

Funding information
Funding was provided by a DFG grant to Prof. Dr O.Strauß (480/12-1). We acknowledge support from the German Research Foundation (DFG) and the Open Access Publication Fonds of the Charite—Universitätsmedizin Berlin

Abstract

The *BEST1* gene product bestrophin-1, a Ca^{2+}-dependent anion channel, interacts with $Ca_V1.3$ Ca^{2+} channels in the retinal pigment epithelium (RPE). *BEST1* mutations lead to Best vitelliform macular dystrophy. A common functional defect of these mutations is reduced trafficking of bestrophin-1 into the plasma membrane. We hypothesized that this defect affects the interaction partner $Ca_V1.3$ channel affecting Ca^{2+} signaling and altered RPE function. Thus, we investigated the protein interaction between $Ca_V1.3$ channels and bestrophin-1 by immunoprecipitation, $Ca_V1.3$ activity in the presence of mutant bestrophin-1 and intracellular trafficking of the interaction partners in confluent RPE monolayers. We selected four *BEST1* mutations, each representing one mutational hotspot of the disease: T6P, F80L, R218C, and F305S. Heterologously expressed L-type channels and mutant bestrophin-1 showed reduced interaction, reduced $Ca_V1.3$ channel activity, and changes in surface expression. Transfection of polarized RPE (porcine primary cells, iPSC-RPE) that endogenously express $Ca_V1.3$ and wild-type bestrophin-1, with mutant bestrophin-1 confirmed reduction of $Ca_V1.3$ surface expression. For the four selected *BEST1* mutations, presence of mutant bestrophin-1 led to reduced $Ca_V1.3$ activity by modulating pore-function or decreasing surface expression. Reduced

Abbreviations: Ano2, anoctamin-2; *BEST1*, human gene encoding the Cl channel bestrophin-1; BVMD, Best vitelliform macular dystrophy; $Ca_V1.3$, pore-forming L-type Ca^{2+} channel subunit of the $Ca_V1.3$ subtype; CHO-K1 cells, Chinese hamster ovary cells K1; c-myc, myelocytomatose gene; DC-electroretinogram, direct current electroretinogram; DMEM, Dulbecco's modified Earle's medium; EOG, electro-oculogram; FCS, fetal calf serum; IP, immunoprecipitation; iPSC, induced pluripotent stem cells; NEDD4, neural precursor cell expressed developmentally down-regulated gene-4; PCC, Pearson's correlation coefficient; PPA2, protein phosphatase-A2; P/S, penicillin, streptomycin; PxxP, proline-rich binding motif; RPE, retinal pigment epithelium; SH3, src-homology domain 3.

Nadine Reichhart and Olaf Strauß are equally contributed to this work.

[Correction added on November 13, 2020 after first online publication: Projekt Deal funding statement has been added.]

$Ca_V1.3$ activity might open new ways to understand symptoms of Best vitelliform macular dystrophy such as reduced electro-oculogram, lipofuscin accumulation, and vision impairment.

KEYWORDS

bestrophin-1, $Ca_V1.3$, retinal degeneration, RPE, surface expression

1 | INTRODUCTION

Best vitelliform macular dystrophy (BVMD) is an autosomal dominant, progredient visual impairment resulting of mutations in the *BEST1* gene.[1-3] *BEST1* encodes bestrophin-1, a protein mainly localized to the basolateral membrane of the retinal pigment epithelium (RPE).[4-6] Since the RPE is a close interaction partner of photoreceptors and responsible for maintaining photoreceptor structure and function,[7] it is hypothesized that mutations in *BEST1* lead to impairment of RPE function and subsequently to photoreceptor loss.[5,8] Hallmarks of the disease are a reduced light-peak in the patient's electrooculogram (EOG)[3-5,8,9] and characteristic alterations in the central retina, vitelliform lesions, accompanied by accumulation of lipofuscin in the RPE.[3,10]

Bestrophin-1 has been described as Ca^{2+}-dependent and volume-activated Cl^- channel.[4,11,12] In heterologous expression, mutant bestrophin-1 shows loss of function due to loss or reduction of plasma membrane trafficking.[13-16] Analysis of human retina sections with defined *BEST1* mutations verified this patho-mechanism at the patient's level.[17] The mutation-dependent loss of basolateral Cl^- conductance might explain the reduced light-peak in the patients' EOG because this signal results from light-dependent activation of basolateral Cl^- channels in the RPE and subsequent depolarization of the basolateral membrane.[4,5,9] Furthermore, a direct loss of Cl^- and water transport or its disturbed regulation might explain the recently detected microdetachments in the retina of a dog bestrophinopathy model that could be cured by gene therapy.[18] As mutant bestrophin-1 in the dog model and human mutant bestrophin-1 have the trafficking defect in common, it is likely that patients with *BEST1* mutations display a reduced Cl^- and water transport like in dog models. Using iPSC-generated RPE from patients with *BEST1* mutations showed a reduction in the phagocytosis of photoreceptor outer segment membranes,[19-21] a process that is essential for the renewal process of the photoreceptors and might explain the accumulation of lipofuscin. This can also result from a reduced activity of the volume-activated Cl channel function because the phagocytosis process requires an efficient volume regulation.[22] Furthermore, also the recently reported changes in the RPE apical surface in canine bestrophinopathy support a phagocytosis defect as a loss of RPE function leading to retinal degeneration.[8,23]

In addition to the loss of Cl channel activity, a disturbed interaction of mutant bestrophin-1 and its interaction partners contributes to the chain of events leading to macular dystrophy. Due to the considerable number of possible interaction partners for bestrophin-1, Johnson et al[5] concluded that bestrophin-1 is a multifunctional protein. The PxxP motifs at the bestrophin-1 C-terminus permit potential interaction with all SH3 domain-containing proteins.[24-26] Some of the interaction partners and data from cell and animal models indicate that bestrophin-1 multifunction contributes to intracellular Ca^{2+} signaling in RPE cells by either modulating Ca^{2+} conductance of the plasma membrane and/or the Ca^{2+} content of cytosolic Ca^{2+} stores.[24-34] Thus, mutation-dependent alterations in intracellular Ca^{2+}signaling as a cause for RPE malfunction and subsequent disturbance of photoreceptor maintenance represent an attractive alternative hypothesis to that of the loss of Cl channel activity The observation that *Best1*$^{-/-}$ mice do not show reduction in RPE Ca^{2+}-dependent Cl channel activity or a reduced light-peak amplitude of the DC ERG that is comparable with the human EOG supports this hypothesis.[29]

Modulation of plasma membrane Ca^{2+} conductance occurs by physical bestrophin-1 and L-type Ca^{2+} channel interaction that is based on bestrophin-1 binding to Ca^{2+} channel β-subunits via coupling of PxxP-motifs SH3 domain.[24-26] The interaction between bestrophin-1 and β-subunits modulates the surface expression and pore function of the main pore forming L-type Ca^{2+} channel subunit in the RPE, the $Ca_V1.3$ subunit.[25,26] Thus, it is to speculate that mutant bestrophin-1 influences the L-type channel activity by reduction of $Ca_V1.3$ surface expression and modulation of pore function. This hypothesis is supported by the fact that $Ca_V1.3$ knockout mice, β4-subunit knockout mice or mice with systemically applied L-type channel blockers show reduced light-peaks in the DC-electroretinogram and thus, reproduce the phenotype of patients with BVMD.[29,33,35] Also in human subjects the systemic application of L-type channel blockers reduces the EOG light peak.[36] Furthermore, in vivo analysis of phagocytosis regulation in $Ca_V1.3$ knockout mice and in vitro analysis of phagocytosis by RPE cells reveal an essential role of L-type channels.[37]

Therefore, we investigated the effect of mutant bestrophin-1 on L-type channels: changes in bestrophin-1/β-subunit protein/protein interaction, biophysical properties of L-type channels in the presence of mutant bestrophin-1 and the subcellular localization of $Ca_V1.3$ in the presence of both WT- and mutant bestrophin-1 in polarized epithelia.

2 | METHODS

2.1 | Plasmids and vectors

The following plasmids/vectors for the $Ca_V1.3$ channels expression were used according to 1. Human bestrophin-1, BEST1 [Homo sapiens; NM_004183], hBest-GFP-pCDNA3 (C-terminal EGFP-tagged human bestrophin), hBest-pcDNA3.1 2. calcium channel, voltage-dependent, β4-subunit (Rattus norvegicus; Gene ID 25297 and 58942); depending on experimental conditions tagged either with His or c-Myc), and β4-pCDNA3; 3. Cacna1d, calcium channel, voltage-dependent, L-type, α1D subunit $Ca_V1.3$ (Homo sapiens: NM_000720.2); 4. α2δ1-pcDNA3 (Gene ID 776), 5. EGFP pcDNA3 and pEGFPN1 reporter plasmid were used as transduction control. Ca^{2+} channel constructs were provided by Prof. Striessnig (Innsbruck, Austria). Human bestrophin-1 constructs were provided by Prof. Weber (Regensburg, Germany) and Prof. Marmorstein (Rochester, USA). Mutant *h*Best-1 pCDNA3 (R218C-, T6P-, F80L-, and F305S-bestrophin-1) were generated by site-directed mutagenesis according to[13] and used depending on experimental design either untagged or with C-terminal GFP tag.

2.2 | Primary cell isolation and cell culture

CHO-K1 cells (ATCC, Wesel, Germany) were grown in DMEM/F12 (Life Technologies, Darmstadt, Germany) supplemented with 10% FCS (Biochrom, Berlin, Germany) und 1% P/S (Biochrom,) at 37°C and 5% CO_2. Cells from passages 3-20 were employed in the present study. Transfection was performed using Lipofectamine 2000 (Thermo Fisher Scientific, Schwerte, Germany) according to the manufacturer's protocol.

2.2.1 | Primary porcine RPE cells

With approval from the authorities (Bezirksamt Mitte von Berlin; approval # 1069/2009) unscalded porcine eyes were obtained from a local slaughterhouse (Schlachthof Färber, Neuruppin, Germany). Porcine eyes were incubated in CO_2 Independent Medium (Life Technologies, Darmstadt, Germany) supplemented with 1% P/S. After two washing steps for 2 minutes in Pursept (Merz Hygiene GmbH, Frankfurt, Germany) an incision was made at the ora serrata to remove the lens and vitreous. Eyecups were filled with sterile CO_2 Independent Medium (supplemented with 1% P/S) and incubated for 15 minutes at RT. After removal of the free-floating retina at the optic nerve, the eyecup was washed two times with TBS. Afterward, eyecups were incubated in a dissociation buffer containing 0.25% Trypsin-EDTA in TBS for 1 hour at 37°C. Dissociated RPE cells were transferred to DMEM (Life Technologies), supplemented with 20% FCS and 1% P/S, After a centrifugation step at 500 *g* for 10 minutes, the RPE cell pellet was dissolved in 1 mL DMEM (with 20%FCS and 1%P/S) per eye and objected to a cell strainer (100 µm pore size; Sigma-Aldrich, Schnelldorf, Germany). 500 000 RPE cells were seeded per 6.5 mm Transwell Polyester Membrane Insert (Corning, Amsterdam, Netherlands). 24 hours before transfection, serum was reduced to 5%.

2.2.2 | Induced pluripotent stem cell (iPSC)-derived human RPE cells

Fibroblasts were obtained from a healthy donor under full consent. Best1 patient fibroblasts were obtained under full patient consent and approved by Columbia University under IRB protocol number AAAF1849. All procedures were in accordance with the Declaration of Helsinki. Fibroblasts were reprogrammed using the non-integrating Sendai virus. Wild-type RPE cells were differentiated from the derived iPSC lines named CRTD1 (Wild-type) and Best1 (Bestrophinopathy patient with D302A point mutation in the *BEST1* gene) according to the protocol describe in.[38] Once differentiated on transwells, Wild-type RPE cells were reseeded on Matrigel-coated coverslips and grown in DMEM-GlutaMaxTM (Thermo Fisher, Schwerte, Germany) supplemented with 20% KnockoutTM Serum Replacement (Thermo Fisher), nonessential amino acids (Thermo Fisher) and 1 mM L-Glutamine and 0.1 mM ß-Mercaptoethanol at 37°C and 5% CO_2 to 60%-90% confluency. 24 hours before transfection, serum concentration was reduced to 5%.

2.3 | Immunoprecipitation and Western Blot

Immunoprecipitation and Western Blot were performed as previously described.[25] Cells were washed 1× with ice-cold TBS and lysed in ice-cold lysis buffer for 15 minutes at 4°C. Lysis

buffer and protease inhibitor were prepared according to.[39] Cells were harvested with scrapers, incubated for 20 minutes at 4°C while shaking and centrifuged at 13 000 *g* for 10 minutes at 4°C. Part of the supernatants was kept as lysate (L). 1 mg/mL of protein was subjected to immunoprecipitation. In cells transfected with $Ca_V1.3$, β4-His, and bestrophin-1, β4-His was precipitated using HisPur Cobalt beads (Thermo Scientific). For precipitation of $Ca_V1.3$, Protein G Agarose (Thermo Scientific) in conjunction with an anti-$Ca_V1.3$ antibody (Alomone labs, Jerusalem, Israel) was applied. After incubation overnight on a rotating wheel at 4°C, the not bound (NB) fraction was stored, and samples were washed three times with lysis buffer. After incubation at 37°C for 40 minutes while shaking in loading buffer, the samples were subjected to SDS page (8%-12% SDS gel). After transfer, the membranes were blocked in 5% milk powder in TBS-Tween 20 for 30 minutes and incubated with the primary antibody against bestrophin-1 (see Table 1) overnight at 4°C while shaking. After incubation of the membranes with the species-appropriate secondary antibody, Chemiluminescence was detected by Clarity Western ECL Substrate (Biorad, Munich, Germany). Images were analyzed with a ChemiDoc XRS imager (Biorad).

2.4 | Quantification of co-immunoprecipitation efficacy

Densitometry analysis of co-immunoprecipitation efficacy was carried out using the Gel Analysis Tool of ImageJ Software (National Institute of Health, USA). The efficacy of co-immunoprecipitations was determined by calculating the relative density values of IP-lane in relation to the L-lane as a control sample.

2.5 | Microinjection and patch clamp

2.5.1 | Microinjection of $Ca_V1.3$ subunits and bestrophin-1

Microinjection was performed as previously described.[26] In short, CHO-K1 seeded on 15 mm coverslips were microinjected using an automated FemtoJet (Eppendorf, Hamburg, Germany) with FemtoTip (Eppendorf) capillaries. The injector was moved by an InjectMan N2 micromanipulator (Eppendorf). The following combinations of plasmid DNA (50 ng/μL for each construct) were injected into the cells: $Ca_V1.3$-subunit α1D, α2δ, β4, WT-bestrophin-1 or the mutations R218C-, T6P-, F80L-, and F305S-bestrophin-1 together with GFP to enable identification of injected cells. Subsequently, cells were incubated overnight at 30°C, and transferred to 37°C the next day.

2.5.2 | Whole-cell patch clamp

Patch Clamp experiments were performed as described in.[25] Mean capacity of the cells was 21.79 ± 0.98 pF (n = 50). To measure ionic currents through L-type channels, we used extracellular 10 mM Ba^{2+} as charge carrier and depolarized the cells from a holding potential of −70 mV to + 20 mV in 10 voltage-steps increases in voltage-amplitude by 10 mV for 50 ms.

2.6 | Immunocytochemistry (ICC) in CHO-K1

For ICC of CHO-K1 on coverslips were fixed with 4% PFA in TBS for 10 minutes. After a permeabilization step (5% Triton X-a00 in TBS) for 10 minutes, unspecific binding sites were blocked by 5% BSA in TBS for 20 minutes. Primary antibody incubation (see Table1) was performed overnight at 4°C. Species appropriate secondary antibodies conjugated with Alexa Fluor 488, 546, 633, or 647 (Life Technologies, Germany) were incubated for 1 hour at room temperature and diluted 1:5000.

2.7 | ICC in primary RPE cells

After 24 hours of transfection, RPE cells were fixed with 4% PFA for 10 minutes, and permeabilized with 5% TritonX100 in TBS for 10 minutes. For blocking unspecific epitopes, cells were incubated in a 5% BSA in TBS solution for 40 minutes at room temperature. Primary antibodies (see Table 1) were applied in 0.8% BSA in TBS solution overnight at 4°C. Species appropriate secondary antibodies were incubated for 1 hour at room temperature. Nuclei were stained with DAPI (1:5000, Sigma) for 10 minutes and cell filter were embedded in Fluorescence Mounting Medium (Dako, Germany). Detection of expression was performed by a confocal microscope (LSM 510, Zeiss, Göttingen, Germany). Data were analyzed by ZEN Software (Zeiss 2009, Germany). Confocal images were analyzed and quantified by ImageJ Software (National Institute of Health, USA).

2.7.1 | Pearson`s correlation coefficient (PCC)

The analysis of correlation (as a measure of colocalization) of $Ca_V1.3$ or Best-1 with the plasma membrane marker, ß-catenin, or $\alpha_5\beta_1$ integrin was calculated with the Plugin JACoP of ImageJ (National Institute of Health, USA).) by measuring PCC. At least n = 4 and maximal n = 23 cells were analyzed.

TABLE 1 Primary antibodies

Primary antibody	Detection in	Dilution	Company
Mouse anti bestrophin-1	WB, ICC	1:500	Abcam
Goat anti-GFP-FITC	ICC	1:200	Abcam
Rabbit anti-His	ICC, WB	1:500	Abcam
Rabbit anti-c-myc	ICC, WB	1:200	Abcam
Mouse anti-c-myc	ICC, WB	1:500	Hybridoma Bank
Rabbit anti-$Ca_V1.3$	ICC, WB	1:250	Alomone labs
Goat anti-$Ca_V1.3$	ICC	1:500	SantaCruz
Rabbit anti-$\alpha_5\beta_1$-integrin	ICC	1:250	Biorbyt
Mouse anti-β-catenin	ICC	1:100	Cell signalling
Mouse anti-β-actin	WB	1:5000	Sigma-Aldrich
Goat anti mouse HRP	WB	1:5000	GE Healthcare

2.7.2 | Apical-basolateral orientation in polarized pRPE cells

In polarized cells, bestrophin-1 is expressed in the basolateral membrane. To analyze if mutant bestrophin-1 is expressed basolateral or apical in pRPE cells confocal z-stacks (n = 6) were analyzed in a blinded fashion by using a score (1: basolateral localization; 2: apical localization). Values were normalized to WT-bestrophin-1.

2.8 | Statistical analysis

All experiments were repeated three times. *n* depicts the number of cells included in the statistic evaluation. Results are expressed as mean ± SEM. Statistical differences are calculated using two-tail ANOVA test, *P*-values lower than .05 were considered statistically significant. All calculations were performed with GraphPad Prism (GraphPad Software Inc, USA) or Sigma Plot (Systat, Erkrath, Germany).

3 | RESULTS

To study the effects of mutant bestrophin-1 on L-type Ca^{2+} channel properties we selected four *BEST1* mutations, each of them representing a mutational hotspot for the disease: T6P-, F80L-, R218C-, F305S-bestrophin-1. For analysis, we first investigated the protein/protein interaction of bestrophin-1 with $Ca_V1.3$ subunits, then the resulting changes in the L-type channel activity and finally the subcellular localization and co-localization of bestrophin-1 and $Ca_V1.3$ in polarized epithelia.

3.1 | Physical interaction of $Ca_V1.3$ with bestrophin-1 mutations

Immunoprecipitation experiments were performed in CHO-K1 cells that heterologously express the L-type channel subunits $Ca_V1.3$ (260 kDa) and β4 (55 kDa) together with different bestrophin-1 constructs. We used β4-subunit because it is the predominant β-subunit in the RPE and β4-subunit knockout reproduces the phenotype of patients with Best vitelliform macular degeneration, the reduction in the light peak.[35] Precipitation of β4 by an antibody against his-tag co-immunoprecipitates β4-subunits and WT-bestrophin-1 in a comparable manner as published earlier (Figure 1).[26] Also the mutant bestrophin-1 F80L, R218C, and F305S showed reliable co-immunoprecipitation with β4-subunits (successful in all conducted experiments) but with, however, lower precipitation efficiency (Figure 1F). These data were retested by indirect immunoprecipitation, where the $Ca_V1.3$/β4 complex was precipited by an antibody against $Ca_V1.3$ and the precipitates were analysed for co-precipitation of bestrophin-1 (Figure S1). Immunoprecipitation of the $Ca_V1.3$-subunit showed comparable results in terms of co-immunoprecipitation efficacy of wild-type bestrophin-1. Expression of the mutants, however, resulted in the loss of co-immunoprecipitation in some experiments. In 2 out of 3 immunoprecipitations of $Ca_V1.3$, R218C-bestrophin-1, and F305S, and in 1 out of 3 F80L-bestrophin-1 could be detected (Figure S1). In case of the mutant T6P-bestrophin-1, only 1 of 6 immunoprecipitations showed reliably detectable co-immunoprecipitation of β4-subunits with T6P-bestrophin-1 (Figure 1). The same was observed when the $Ca_V1.3$/β4 complex was precipitated. Here, also 1 in 6 precipitations showed a co-precipitation with T6P mutant bestrophin-1. Thus, we assume that T6P can bind to β4-subunits, but the binding efficiency is too weak

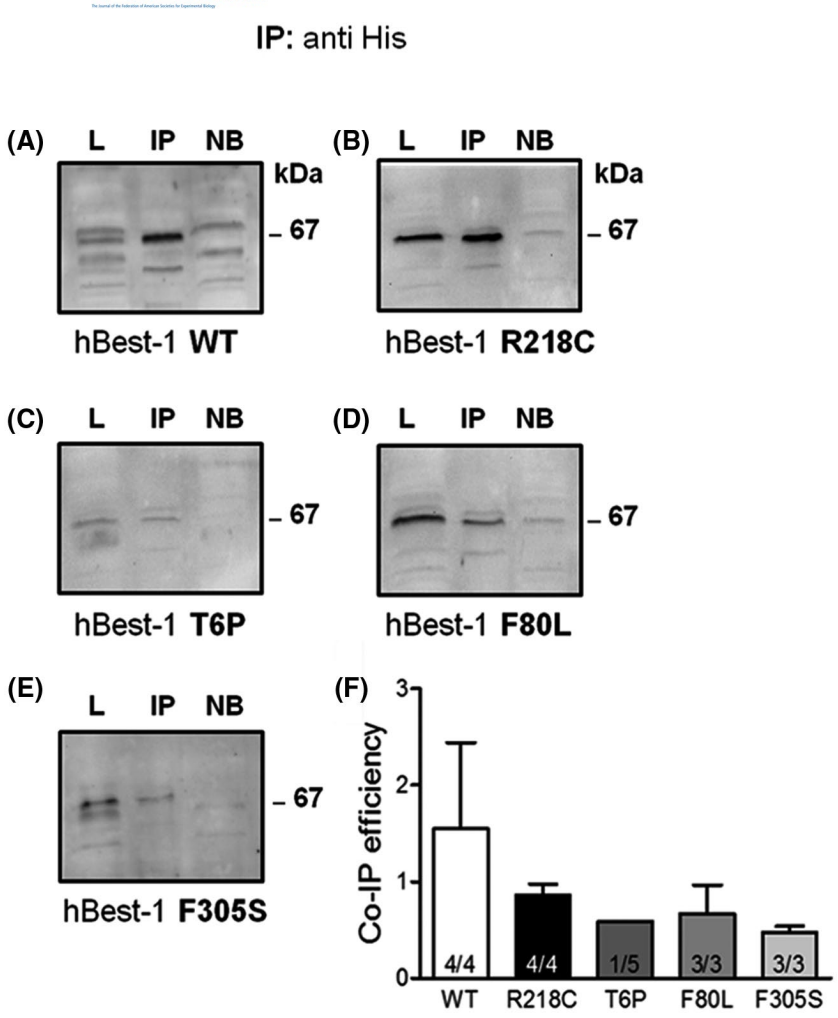

FIGURE 1 Physical interaction of calcium channels subunit β4 with bestrophin-1 in CHO-K1. Transfection of $Ca_V1.3$, his-tagged β4-subunit and bestrophin-1 (WT-bestrophin-1 A, R218C-bestrophin-1 B, T6P-bestrophin-1 C, F80L-bestrophin-1 D, F305S-bestrophin-1 E). Immunoprecipitation of 6xhis-tagged β4, western blot of L (lysate), IP (immunoprecipitation), and NB (not-bound) against bestrophin-1; protein size is given in kDa (bestrophin-1.67 kDa). F, bar chart illustrating co-immunoprecipitation efficacy of β4-subunit and bestrophin-1. The first number illustrates successful co-immunoprecipitation and second number illustrates the number of trials

to generate reproducible results co-immunoprecipitations. In summary, these data indicate a physical interaction between Ca^{2+} channel subunits and all mutant bestrophin-1.

3.2 | Subcellular localization of $Ca_V1.3$ in the presence of bestrophin-1-mutations in CHO-K1 cells

The common effect of all *BEST1* mutations investigated so far is a loss or reduction of bestrophin-1 surface trafficking. To investigate whether alterations of trafficking of mutant bestrophin-1 also reduce the plasma membrane localization of $Ca_V1.3$ channels in CHO-K1, co-localization of bestrophin-1 mutants with $Ca_V1.3$ and subcellular localization of these proteins were analyzed by ICC. $\alpha_5\beta_1$-integrin served as a cell surface marker in CHO-K1. Transfection of $Ca_V1.3$-subunit, β4-subunit, and WT bestrophin-1 resulted in co-localization of $Ca_V1.3$ and bestrophin-1 in the plasma membrane. R218C-bestrophin-1 showed similar results for co-localization of $Ca_V1.3$ and bestrophin-1 in the plasma membrane. F80L-bestrophin-1 showed diffuse staining both in the plasma membrane and the cytosol. In the presence of T6P-bestrophin-1, which was predominantly localized to the cytosol, or in the presence of the patchy dot-like cytosolic F305S-bestrophin-1, also $Ca_V1.3$ was localized to the cytosol (Figure 2A). PCC was significantly reduced in the presence of the mutants T6P-, F80L-, and F305S-bestrophin-1, both for $Ca_V1.3$ surface expression (Figure 2B left) and $Ca_V1.3$-bestrophin-1 interaction (Figure 2C). Distribution analysis of R218C-bestrophin-1 resulted in values comparable to that of WT-bestrophin-1 (Figure 2B,C).

3.3 | Influence of mutant bestrophin-1 on $Ca_V1.3$ channel activity in CHO-K1 cells

After observing reduced membrane expression of $Ca_V1.3$ in the presence of T6P-, F80L-, and F305S-bestrophin-1, the influence of mutant bestrophin-1 on L-Type channel activity was examined by whole cell patch clamp recordings. CHO-K1 were microinjected with L-type channels-subunits ($Ca_V1.3$, α2δ, β4 for obtaining ionic currents through the L-type channel) and bestrophin-1. The presence of mutant bestrophin-1 reduced the maximum Ba^{2+} current density

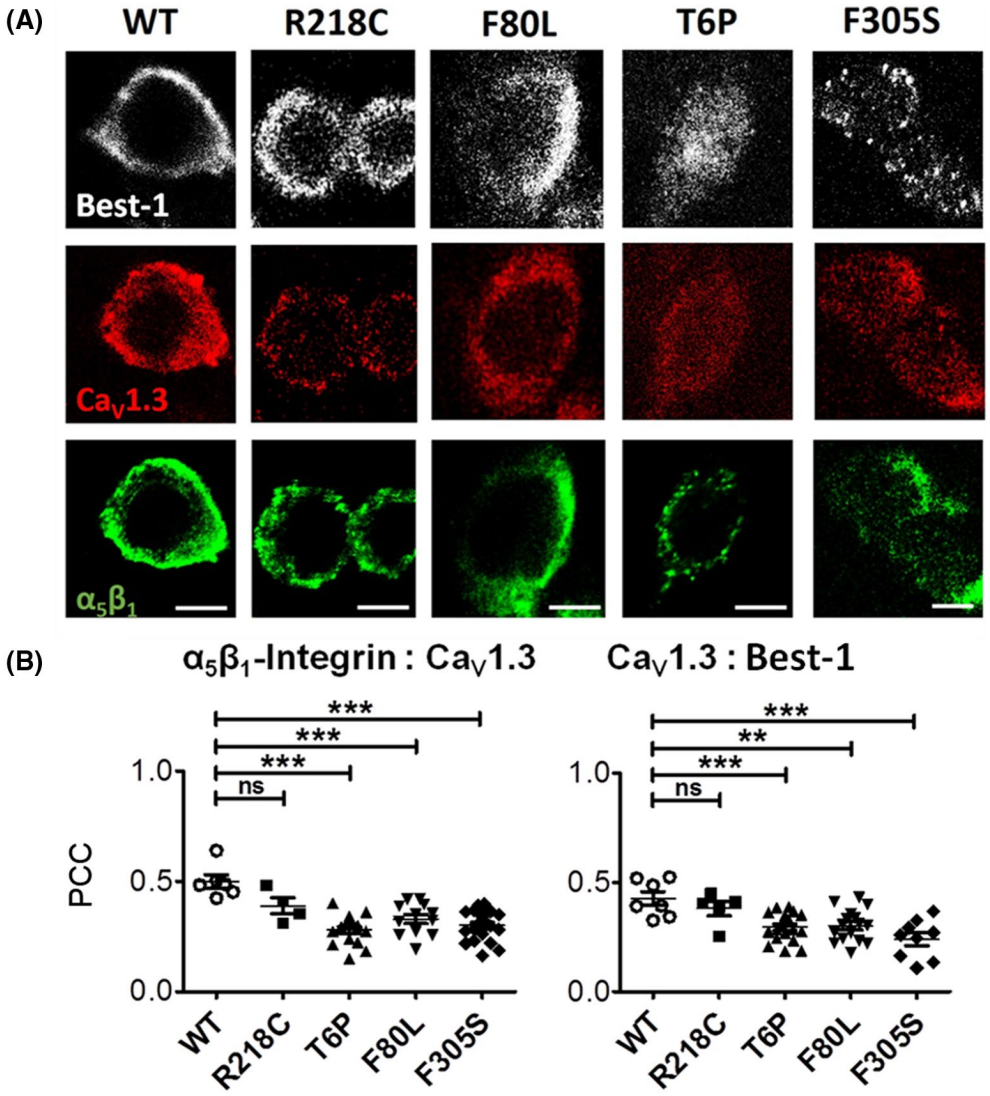

FIGURE 2 Subcellular localization of $Ca_V1.3$ and bestrophin-1 in CHO-K1. A, confocal images of CHO-K1 transfected with $Ca_V1.3$, β4-subunit and bestrophin-1 (columns show WT and the different point mutations). Upper panel: staining against bestrophin-1 (white) middle panel staining against CaV1.3 (red); lower panel: staining against the plasma membrane marker $\alpha_5\beta_1$-integrin (green). B, scatter plot of the PCC of $\alpha_5\beta_1$-integrin and $Ca_V1.3$ (left) and $Ca_V1.3$ to bestrophin-1 (right). n = 4-23; $^{**}P < .01$, $^{***}P < .001$

at a membrane potential of 10 mV compared to that in the presence of WT-bestrophin-1 (Figure 3A). This reduction, however, was only significant for F80L-bestrophin-1 and F305S-bestrophin-1 (Figure 3B,D). Furthermore, F80L-bestrophin-1 and F305S-bestrophin-1 also showed significant alterations of voltage-dependence. To analyze voltage-dependence of L-type channel currents, current-voltage plots of Ba^{2+} currents were normalized to the voltage of maximal currents and fitted using the Boltzmann equation to obtain slope factor of the curve (k_{act}) and voltage of half-maximal activation ($V_{0.5}$). The half-maximum activation $V_{0.5}$ was shifted toward more positive values in the presence of F80L-bestrophin-1 and F305S-bestrophin-1. The slope factor k_{act} was significantly smaller in the presence of these two mutants (Figure 3C,D). Activation kinetics remained unchanged in the presence of all mutants (Table 2, Figure S2).

3.4 | Influence of mutant bestrophin-1 on endogenously expressed bestrophin-1 and $Ca_V1.3$ in polarized RPE

To validate the results obtained in CHO-K1, the interaction of endogenously expressed bestrophin-1 with transfected mutant bestrophin-1 was assessed in confluent polarized primary cultures of porcine RPE cells (pRPE).

pRPE were grown on filters to establish the cell polarity with endogenous expression of bestrophin-1 and $Ca_V1.3$ (Figures 4-6). Transfected bestrophin-1 constructs

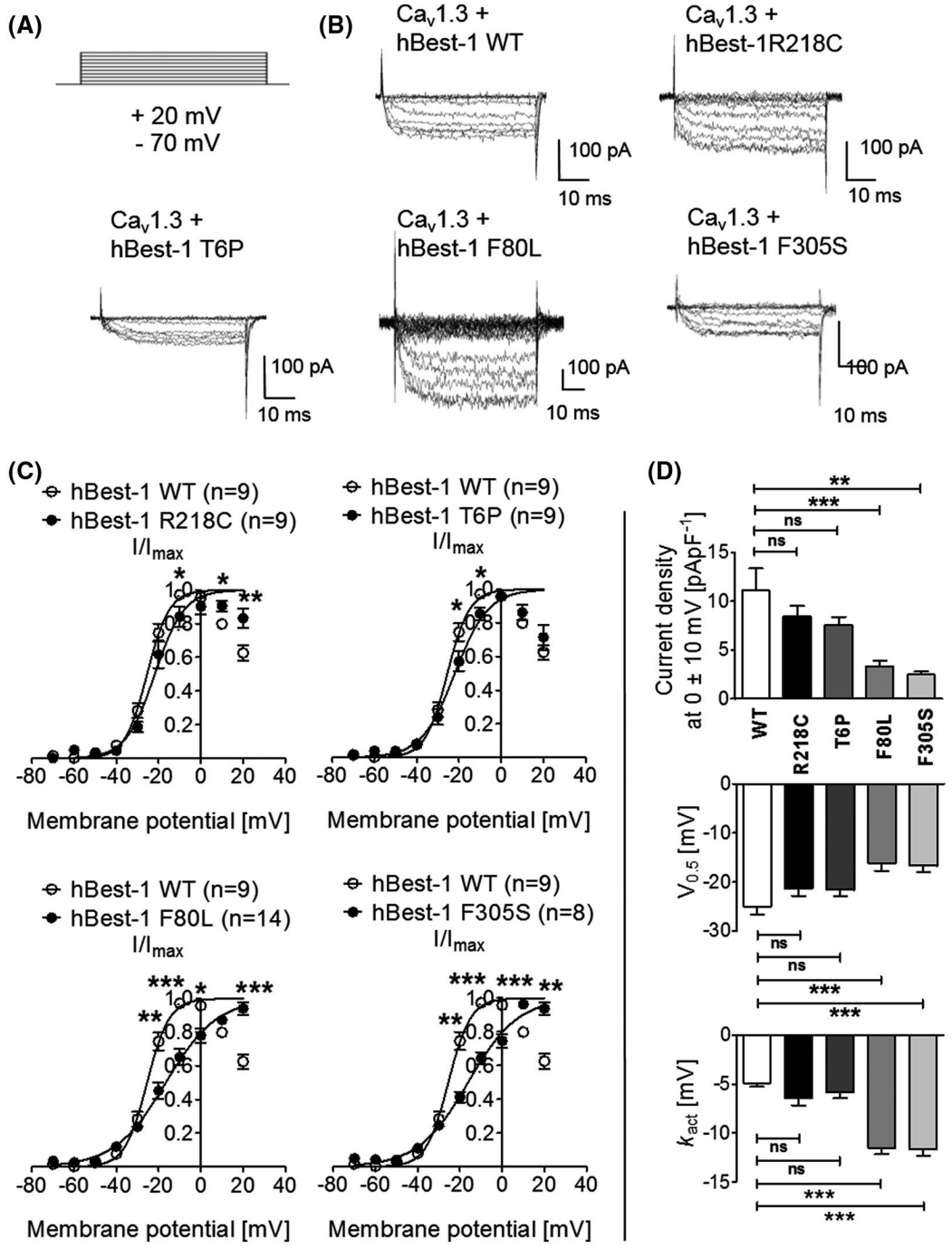

FIGURE 3 Influence of mutant bestrophin-1 on $Ca_V1.3$ channel function in CHO-K1. A, step-wise depolarization from a holding potential of −70 mV to + 20 mV. B, Ba^{2+} currents in a cell expressing $Ca_V1.3/\beta_4/\alpha_2\delta$ and WT-bestrophin-1 or mutant bestrophin-1 (R218C-, T6P-, F80L-, F305S-bestrophin-1). C, current-voltage plot of Ba^{2+} currents normalized to the voltage of maximal currents (fitted with Boltzmann equation) in presence of WT-, R218C-, T6P-, F80L-, and F305S-bestrophin-1. D, Upper panel: Bar chart representing the maximum current density for cells transfected with either wildtype- or mutant (R218C-, T6P-, F80L-, F305S-) bestrophin-1. Comparison of parameters from Boltzmann fits: potential of half-maximal activation ($V_{0.5}$, middle panel) and slope factor ($k_{act,}$ lower panel); $*P < .05$; $**P < .01$, $***P < .001$

were identified by their YFP or c-Myc-tag (green channel), whereas total bestrophin-1 (transfected and endogenously expressed) was visualized by an anti-bestrophin-1 antibody (red channel). β-Catenin served as a membrane marker in pRPE (blue channel) (Figure 4A). When polarized pRPE cells were transfected with WT-bestrophin-1, we observed co-localization of both, transfected and total, bestrophin-1 in the plasma membrane. Thus, the transfection with WT-bestrophin-1 did not affect the trafficking behavior of endogenously expressed bestrophin-1. Transfection with R218C-bestrophin-1 showed a similar pattern, although the PCC was slightly reduced. T6P-, F80L-, and

TABLE 2 Summary of basic electrophysiological characterization of $Ca_V1.3$ currents in the presence of bestrophin mutations in CHO-K1

Transfection: $\alpha_1D/\alpha_2\delta_1/\beta_4$ + hBest1X	$V_{0.5}$ [mV]	$k_{act\ [mV]}$	Activation time constant at 0 mV [ms]	Current density at V_{max} [pA/pF]
hBest1 WT (n = 9)	−25.1 ± 1.53 (n = 9)	4.90 ± 0.38 (n = 11)	1.83 ± 0.05 (n = 3)	−11.1 ± 2.26 (n = 9)
hBest1 R218C (n = 10)	−21.4 ± 1.45 (n = 10)	6.43 ± 0.79 (n = 8)	2.55 ± 0.55 (n = 2)	−8.46 ± 1.07 (n = 9)
P-value	.0961	.0687	–	.3062
hBest1 T6P (n = 9)	−21.6 ± 1.28 (n = 9)	5.86 ± 0.57 (n = 8)	2.30 ± 0.36 (n = 3)	−7.54 ± 0.09 (n = 9)
P-value	.0984	.1630	–	.1596
hBest1 F80L (n = 14)	−16.1 ± 1.59 (n = 14)***	11.5 ± 0.64 (n = 14)***	2.05 ± 0.05 (n = 2)	−3.35 ± 0.58 (n = 14)***
P-value	.0009	.0001	–	.0006
hBest1 F305S (n = 8)	–16.7 ± 1.36 (n = 8)**	11.6 ± 0.68 (n = 8)***	2.1 ± 0.10 (n = 2)	–2.49 ± 0.33 (n = 8)***
P-value	.0010	.0001	–	.0029

*$P < .05$; **$P < .01$; ***$P < .00$.

F305S-bestrophin-1 transfection showed a substantial reduction of co-localization with β-Catenin and diffuse or patchy expression of both endogenous and transfected bestrophin-1 all over the cytosol (Figure 4A,B).

The apical to basal polarity of mutant bestrophin-1 in pRPE cells was quantified by analysis of z-stacked confocal images. Application of a score with one depicting basolateral localization and two apical localization, showed a predominantly basolateral expression of WT-bestrophin-1 and R218C-bestrophin-1 whereas T6P-bestrophin-1 and F305S-bestrophin-1 were localized at the apical side of the cells. F80L-bestrophin-1 showed neither basolateral nor apical preference (Figure 4C). Taken together, mutant bestrophin-1 showed a dominant effect over WT-bestrophin-1 leading to reduced surface expression.

In a next step, the influence of bestrophin-1 on $Ca_V1.3$ surface expression was assessed by the PCC analysis. Transfection of R218C, T6P, F80L, or F305S-bestrophin-1 led to a reduction of correlation between the surface marker β-Catenin and $Ca_V1.3$, (Figure 5A,B).

To determine the effect of mutant bestrophin-1 on $Ca_V1.3$-bestrophin-1 interaction, subcellular localization of transfected, and total bestrophin-1 was compared to that of endogenously expressed $Ca_V1.3$ (Figure 6A,B). Cells transfected with WT-, R218C-, F80L-, and F305S bestrophin-1 showed co-localization of transfected bestrophin-1 and $Ca_V1.3$, whereas T6P-bestrophin-1 mostly showed intracellular distribution co-localizing partly with $Ca_V1.3$ (black bars). Staining of total bestrophin-1 showed co-localization of bestrophin-1 with $Ca_V1.3$ only in the presence of WT-, R218C-, and F80L-bestrophin-1 (graybars).

The results in pRPE cells were similar to the results in human iPSC-derived RPE cells grown under polarized conditions. In accordance to pRPE, transfection of T6P-bestrophin-1 led to a significant reduction of plasma membrane expression of both total bestrophin-1 as well as $Ca_V1.3$ whereas R218C-bestrophin-1 revealed similar results compared to WT (Figure 7). Finally, we used the iPSC technology to investigate at least one mutation under non-overexpression conditions when both wild-type and mutant bestrophin-1 were endogenously expressed. iPS cells from a patient of BVMD carrying a D302A mutation were differentiated into confluent monolayers of RPE cells. Localization of bestrophin-1 and $Ca_V1.3$ was investigated by means of ICC . As in the overexpression system, we observed mislocation in the cytosol instead in the plasma membrane of both bestrophin-1 and $Ca_V1.3$ (Figure 7B). Furthermore, co-localization of the two proteins indicate physical interaction of L-type channels and bestrophin-1 pentamers composed of both mutant and WT-bestrophin-1.

In summary, the presence of mutant bestrophin-1 reduces the surface expression of $Ca_V1.3$ channels and (for F80L- and F305S-bestrophin-1) changes at the same time the L-type channel activity in heterologous expression system. Furthermore, the bestrophin-1/Ca^{2+} channel interaction is disturbed, predominantly with T6P- and F305S bestrophin-1. To correlate L-type channel activity and cellular distribution of $Ca_V1.3$, we compared mean values of PCC analysis of $Ca_v1.3$ and $\alpha_5\beta_1$-integrin to maximum current density in the presence of different bestrophin-1 proteins in CHO-K1 (Figure 8A). There was a statistically significant difference only detectable for F305S and F80L, the two mutants that led to very small values in current density. Comparing the results from PCC analysis of $Ca_V1.3$ surface expression in the polarized epithelium (pRPE) with the unpolarized condition (CHO-K1, Figure 8B) showed no significant differences except for F305S-bestrophin-1, the mutation with the smallest PCC in CHO-K1.

4 | DISCUSSION

In this study, we investigated the influence of bestrophin-1 with disease-causing mutations on L-type channels of the

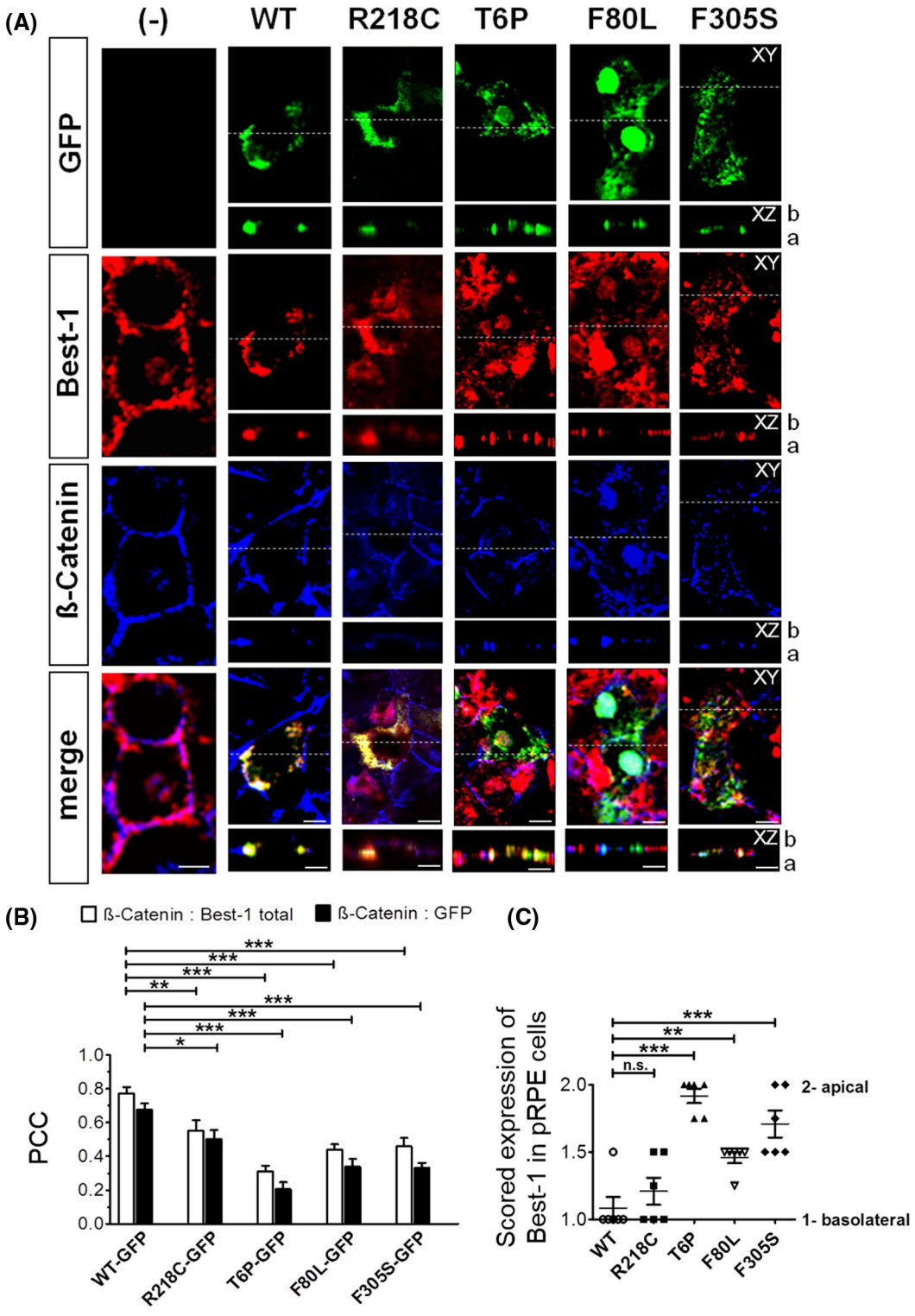

FIGURE 4 Influence of mutant bestrophin-1 on endogenously expressed bestrophin-1 in polarized porcine RPE (pRPE). A, pRPE cells untransfected (first column) or transfected with GFP-tagged WT-or mutant bestrophin-1 stained with antibodies against GFP (green, transfected bestrophin-1, first panel), bestrophin-1 (red, total = transfected and endogenously expressed bestrophin-1, second panel), β-Catenin (blue, surface marker, third panel). Fourth panel shows merge of three panels. B, PCC of β-Catenin and total bestrophin-1 (white bars) or β-Catenin and transfected bestrophin-1(black bars) in the presence of transfected WT- or mutant bestrophin-1 (n = 6-10) C, scatter plot representing apical or basolateral polarity of WT- and mutant bestrophin-1. 1 = basolateral localization, 2 = apical localization. (*$P < .05$; **$P < .01$, ***$P < .001$, scale bar represents 10 μm)

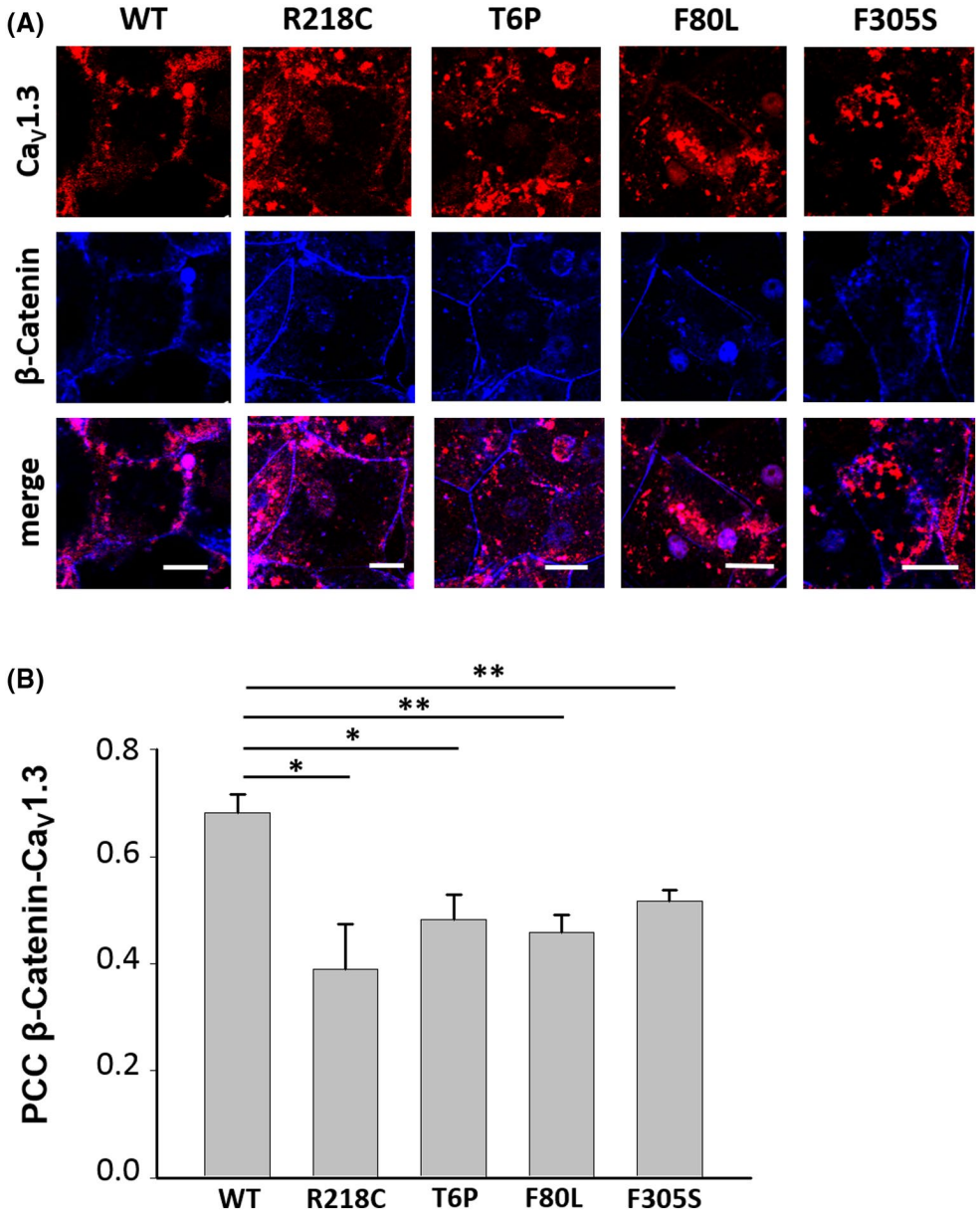

FIGURE 5 Surface expression of $Ca_V1.3$ in the presence of both mutant and endogenous WT-bestrophin-1 in polarized pRPE. A, confocal images of pRPE cells transfected with bestrophin-1 (columns show WT and the different point mutations): staining against $Ca_V1.3$ (red), β-Catenin (blue), and the overlay of all panels (merge). B, PCC analysis of $Ca_V1.3$ and β-Catenin (gray bars); n = 4-16. Whiskers represent standard error of the mean. (*$P < .05$; **$P < .01$, scale bar represents 20 μm)

$Ca_V1.3$ subtype, the predominant L-type channel subtype in RPE cells. We examined four mutations representing the mutational hotspots for Best vitelliform macular degeneration and went from the analysis of molecular interaction of bestrophin-1 with Ca^{2+} channel subunits and of properties of L-type channels in the presence of mutant bestrophin-1 to the assessment of trafficking of bestrophin-1 and $Ca_V1.3$ subunits in polarized porcine or human RPE cells. We found that mutant bestrophin-1 still interacts with Ca^{2+} channel β4-subunits, reduces the L-type channel activity, and prevents trafficking of $Ca_V1.3$-subunits to the plasma membrane.

The goal of this study was to determine the molecular base for the interaction of mutant bestrophin-1 with L-type Ca^{2+} channel subunits and their cellular behavior. Studies of mutant bestrophin-1 in heterologous expression reported data representative for absence of WT-bestrophin-1.[4,13-15,22,40-42] Studies using iPSC-generated RPE cells from patients with BVMD report slightly different results showing that the presence of WT-bestrophin-1 influences the outcome.[19] The patients` iPSC model, however, does not permit differential detection of mutant versus WT-bestrophin-1 and bears the disadvantage that different cell lines from the same iPSC

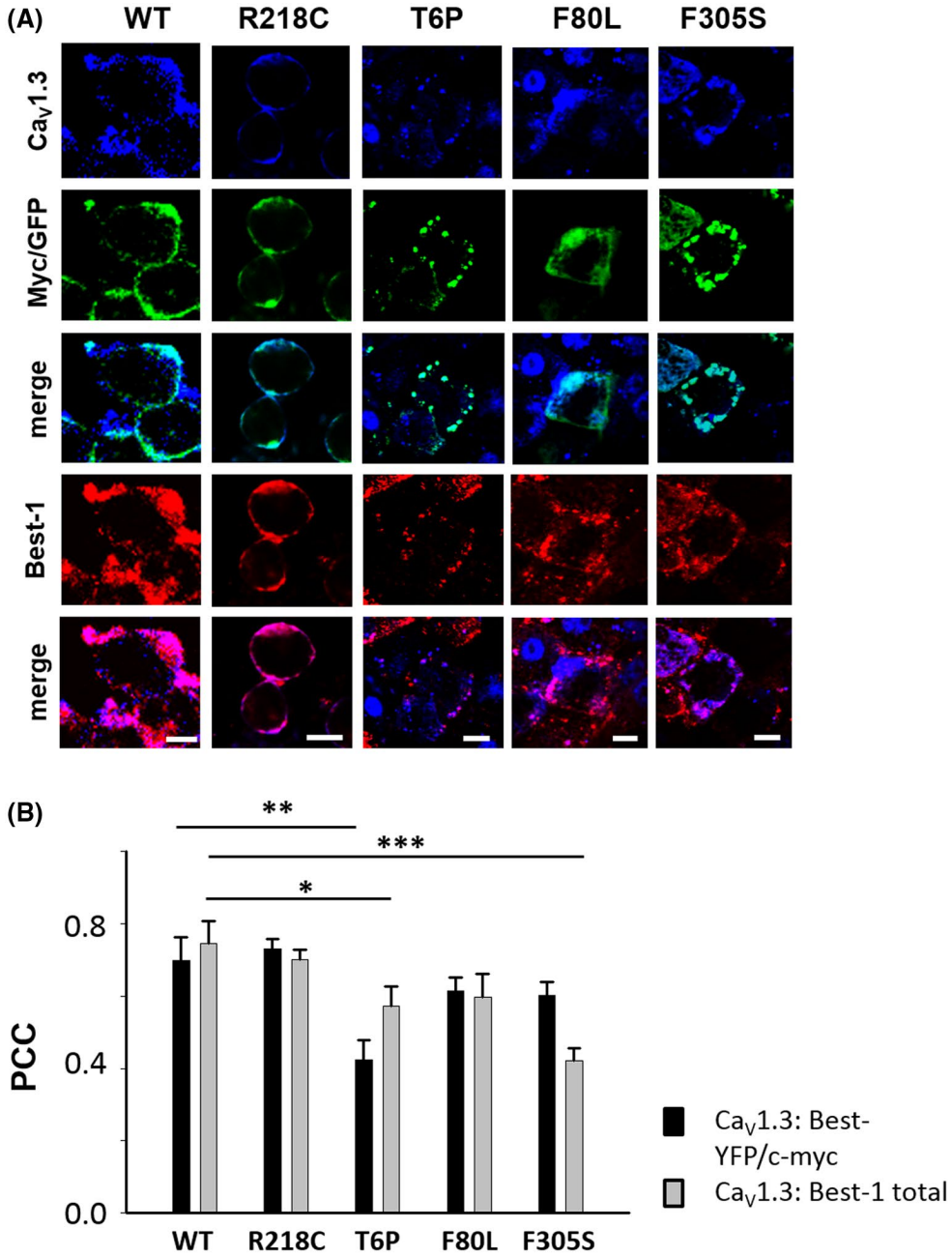

FIGURE 6 Influence of mutant bestrophin on $Ca_V1.3$-bestrophin-1 co-localization in pRPE. A, confocal images of pRPE cells transfected with bestrophin-1 (columns show WT and the different point mutations): staining against mutant bestrophin-1 tagged with GFP or c-Myc (green), $Ca_V1.3$ (blue), the overlay of blue and green, panels (merge); staining against total bestrophin-1 (red), and the overlay of blue and red (merge) C, PCC analysis of $Ca_V1.3$ and GFP-tagged mutant bestrophin-1 (black bars), and $Ca_V1.3$ and total bestrophin-1 (gray bars) n = 7-18 (*$P < .05$; **$P < .01$, ***$P < .001$, scale bar represents 20 μm)

show strong variances. Thus, we used in vitro models based on heterologous transfection selected for specific experimental needs. Heterologous expression in CHO-K1 cells delivers high amounts of proteins and considerably large current amplitudes of L-type channels to examine the molecular base of bestrophin-1/Ca^{2+} channel interaction. Polarized RPE monolayer (primary porcine RPE cultures and iPSC-generated human RPE cells) with endogenous expression of WT-bestrophin-1 and L-type channels transfected with either WT- or mutant bestrophin-1 offer the advantage to study cellular protein and to detect the proportion of transfected bestrophin-1 in total bestrophin-1.

Physical interaction between bestrophin-1 and Ca^{2+} channel β-subunits was successfully studied by means of immunoprecipitation and measurements of the co-immunoprecipitation efficiency.[25,26] We used the same method to investigate the interaction of mutant bestrophin-1 with the Ca^{2+}-channel protein complex formed of $Ca_V1.3$- and

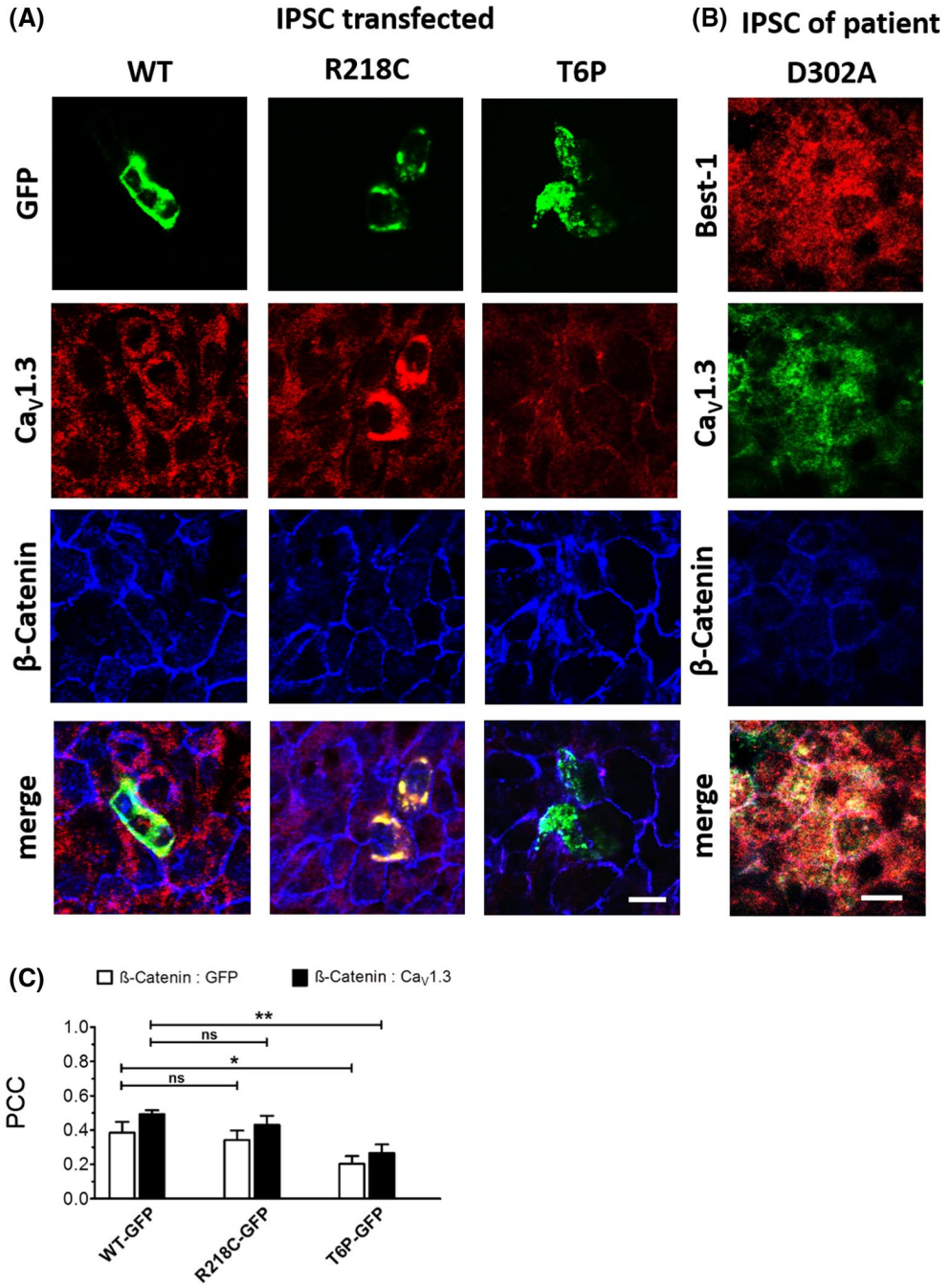

FIGURE 7 Subcellular localization of mutant bestrophin-1 on endogenous $Ca_V1.3$ and endogenous WT-bestrophin-1 in IPSC-derived RPE. A, confocal images of pRPE cells transfected with bestrophin-1 (columns show WT-, R218C-, and T6P-bestrophin-1: staining against mutant bestrophin-1 tagged with GFP (green), $Ca_V1.3$ (red), the plasma membrane marker ß-catenin (blue), and the overlay of all panels (merge). B, confocal images from patient's iPS-generated RPE cells carrying the mutation D302A: stained for Cav1.3 (green), bestrophin-1 (red), β-catenin (blue) C, quantification of surface expression by PCC of ß-catenin to GFP-tagged mutant bestrophin-1 (GFP, white bars) and ß-catenin to $Ca_V1.3$ (black bars), n = 4-6; (*$P < .05$; **$P < .01$, scale bar represents 10 μm)

β4-subunits. $Ca_V1.3$ is the prominent pore-forming L-type Ca^{2+} channel subunit in the RPE, and knockout mice of either $Ca_V1.3$- or β4-subunits show reduced light peaks in DC-electroretinogram[29,35]; a phenotype corresponding to the EOG in Best patients. The co-immunoprecipitation of WT-bestrophin-1 with $Ca_V1.3$/β4-complexes reproduced data that were published earlier.[25,26] All mutant bestrophin-1, however, showed co-immunoprecipitation with the $Ca_V1.3$/β4-complex albeit of reduced efficiency. This result is in accordance with the localization of all mutations at the N-terminal half of bestrophin-1 whereas domains for β-subunit binding are on the C-terminus. Comparable to other expression systems,[13-16,19-21] in CHO-K1, mutant bestrophin-1 showed reduced surface expression. The $Ca_V1.3$ interaction reduces

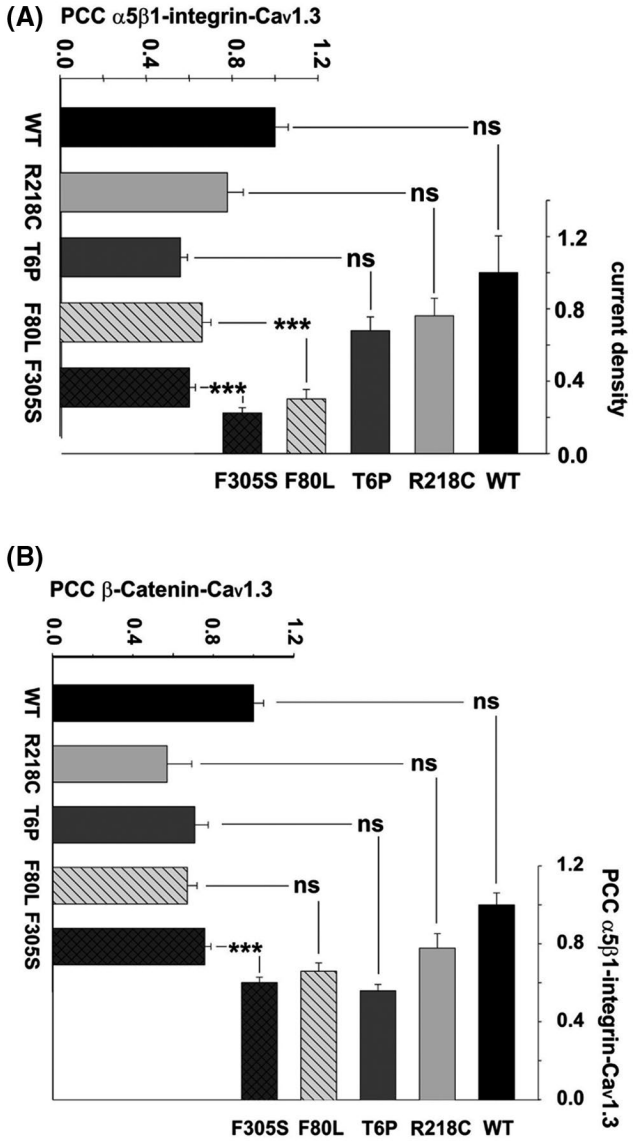

FIGURE 8 Correlation of surface expression and current density of $Ca_V1.3$ in CHO-K1 and pRPE. A, Correlation of data from the current density of L-Type channels (Figure 3D) and surface expression of $Ca_V1.3$ in the plasma membrane of CHO-K1 measured by PCC (Figure 2B, left panel) in the presence of mutant or WT-bestrophin-1. B, Correlation of surface expression $Ca_V1.3$ in the plasma membrane of pRPE cells (Figure 6B) and CHO-K1 (Figure 2B, left panel) measured by PCC in the presence of mutant or WT- bestrophin-1. Data are normalized to WT (*$P < .05$; **$P < .01$, ***$P < .001$)

$Ca_V1.3$ plasma membrane localization as well. The mutation R218C showed no significant effects on either Ca^{2+} channel trafficking or bestrophin-1 trafficking. This corresponds with other publications showing that R218C develops only weak trafficking defects and mild loss of anion permeability. An exception is the mutation T6P that showed weak binding to β4-subunits. Co-immunoprecipitation could only be detected once in six experiments. Patch-clamp analysis of transfected CHO-K1 showed that mutant forms F80L and F305S reduced the maximal current density of L-type channel and shifted the voltage-dependent activation toward more positive potentials. This should result in a further reduction of the L-type channel activity in RPE at physiological voltages. Again, R218C showed no significant effects on L-type channel activity. Surprisingly, although T6P bestrophin-1 reduced the surface expression of $Ca_V1.3$, it did not significantly change L-type channel activity. We explain this observation by two effects. Physiologically WT-bestrophin-1 binding decreases $Ca_V1.3$ currents. Since T6P bestrophin-1 binds very weakly to β-subunits, we expect larger $Ca_V1.3$ currents in the presence of T6P than in the presence of WT-bestrophin-1. Moreover, mutations in bestrophin-1 have severe effects on the protein synthesis machinery. It is likely that T6P non-specifically reduces the surface expression of $Ca_V1.3$ and only mildly affects overall currents due to lack of bestrophin-1-dependent $Ca_V1.3$ inhibition. Comparing the effect of the mutations on channel activity and surface expression, we confirm the correlation of PCC and current density in CHO-K1 for WT, R218C, and T6P; due to very small values for F80L and F305S, the correlation for these mutants is weak. In summary, we conclude that mutant bestrophin-1 affects L-type channels in various ways resulting in an overall reduction of Ca^{2+} channel surface expression. Depending on the mutation, it can even directly influence pore-function by means of voltage-dependence and maximal channel activity.

X-ray structure analysis of bestrophin-1 revealed that it forms pentamers.[43] Since CHO-K1 were transfected with only one specific bestrophin-1, the conclusions obtained are drawn with mutant bestrophin-1 pentamers. These conclusions, however, were further supported in experiments using polarized RPE cells with endogenous WT expression and mutant bestrophin-1 transfection. In control experiments with primary porcine RPE cells, WT-bestrophin-1 transfection did not affect the cellular trafficking of endogenously expressed bestrophin-1. Since we found that the signals from total (includes both endogenously and transfected bestrophin-1) and transfected bestrophin-1 were co-localized, we conclude that endogenously expressed bestrophin-1 and transfected bestrophin-1 form pentamers together. With exception of R218C, transfection with mutant bestrophin-1 dramatically reduced the surface expression of total bestrophin-1 and revealed reduced the surface expression of mutant bestrophin-1 (detected by either GFP-tag or c-Myc-tag). The reduction in the surface expression of total bestrophin-1 is comparable to that of the transfected mutant bestrophin-1 indicating that mutant mutant bestrophin-1 influences the behavior of the wild-type bestrophin-1.

Furthermore, also with exception of R218C, mutant bestrophin-1 lost basolateral distribution. Mutant bestrophin-1 was found either in the middle of the cell (F80L, F305S) or even apical (T6P). Thus, our in vitro models reproduce data

known from the literature using the heterologous expression, iPSC-generated RPE cells from Best patients and from ex vivo analysis of patient's eyes.

Next, we investigated the subcellular localization of endogenously expressed $Ca_V1.3$ subunits in polarized epithelia. Cells of either porcine primary cultures or iPSC-derived RPE that were transfected with WT-bestrophin-1 showed no changes in the plasma membrane localization of the pore-forming L-type Ca^{2+} channel subunit. Thus, the overexpression of bestrophin-1 per se does not influence the behavior of the endogenously expressed bestrophin-1 and the $Ca_V1.3$ subunits. All mutant bestrophin-1 reduced the plasma membrane expression of $Ca_V1.3$ subunits confirming that we could identify a mutation-dependent effect. At least for one mutation we confirmed data from overexpression at a condition where both, the wild-type and the mutant bestrophin-1, were endogenously expressed. We used iPS-derived RPE cells from a patient carrying the D302A mutation, that is very close to the F305S mutation that we have analysed in overexpression system. In these patient's iPS-derived RPE cells, we found predominant cytoplasmic localization of both bestrophin-1 and Cav1.3 L-type channel subunits and a strong co-staining of the two proteins. These data support those derived from overexpression in porcine RPE cells, but in the patient's iPS-RPE cells under dominant negative conditions. Comparing the results from PCC analysis of $Ca_V1.3$ surface expression in polarized and unpolarized condition, showed no significant differences except for F305S, the mutation with the smallest PCC in CHO-K1; thus, the basic findings in unpolarised epithelium complement the data from the polarized condition.

The anion channel function of bestrophin-1 and its changes by disease-leading mutations has been extensively studied. The overall conclusion in these studies is that *BEST1* mutations lead to a loss of anion conductance either due to trafficking defects or to loss of pore function. As the light-peak in the EOG results from activation of Cl channels in the RPE basolateral membrane, these observations deliver an explanation for the patients' phenotype. More recent work indicated that *BEST1* mutations impair phagocytic activity by the RPE, probably by a loss of volume control that leads to lipofuscin accumulation.[19,22] However, the hypothesis that the loss of Cl^- conductance alone might explain the pathology of disease BVMD is insufficient. Mouse models with a knockout of bestrophin-1 or with knock-in of mutations into bestrophin-1 showed no changes in anion conductance.[29,32] This can be explained by the expression of anoctamin-2 (Ano2) in RPE cells.[44] Ano2 is a Ca^{2+}-dependent Cl^- channel that could compensate for the loss of bestrophin-1 in the basolateral membrane. Thus, the reduced light-peak in Best patients results from the dysregulation of Ca^{2+}-dependent Cl^- channels by intracellular Ca^{2+} signaling. Indeed, several lines of evidence suggest a role of bestrophin-1 in Ca^{2+} signaling. Bestrophin-1 interacts with L-type channels or participates in Ca^{2+} signalling from recruitment of intracellular Ca^{2+} stores.[25,26,28,29,42] RPE cells of the W93C knock-in mouse show reduced cytosolic Ca^{2+} amplitudes in response to ATP stimulation.[32]

With $Ca_V1.3$, we have investigated one interaction partner of bestrophin-1. To date, there are more interaction partners of bestrophin-1 known such as phosphatase PPA2 or NEDD4.[5,45,46] The excellent review by Johnson et al[5] discusses bestrophin-1 as a multifunctional protein. Thus, not only the disturbed interaction of mutant bestrophin-1 with Ca^{2+} channel subunits contributes to the chain of events leading to macular dystrophy. In *vivo* studies and in vitro studies, however, point toward the idea that this multifunction regulates Ca^{2+} signalling in the RPE.[5] Our data further support a role of Ca^{2+} signaling in disease. Mutant bestrophin-1 reduces L-type channel activity in different ways due to physical interaction of bestrophin-1/$Ca_V1.3$. Reduction in L-type channel activity can occur by reduction of the number of L-type channel pores in the plasma membrane and/or by shifts in the voltage-dependence that reduce pore activity. Mutant bestrophin-1 forms with WT-bestrophin-1 pentamers resulting in a dominant negative on WT-bestrophin1 and subsequent influence of L-type channel properties even by mutants with low binding efficiency to Ca^{2+} channel β-subunits. The overall loss of L-type channel activity would explain the reduced light-peak in the patient's EOG because either systemic inhibition of RPE L-type channels or knockout of $Ca_V1.3$ channels mice results in reduced light-peaks.[29] Activation of Ano2 in the RPE leads to basolateral membrane depolarization that in turn activates L-type channels.[44] This further increases intracellular Ca^{2+} and Cl channel activity and therefore the light-peak amplitude. In addition, several papers indicate that L-type channels are also involved in the regulation of the phagocytic activity of the RPE in vitro and in vivo.[37,47,48] Thus, a reduction in the L-type channel activity in the RPE might explain the accumulation of lipofuscin in the RPE of patients with Best vitelliform macular dystrophy, too. Enhancement of L-type channel activity might be an important therapeutic target for these patients. However, recent data from a gene therapy study detected a new aspect of Best vitelliform macular dystrophy, such a microdetachments, that occur apart of the reduction of the light peak in the EOG.[18] Thus, mutant-dependent changes in the Ca^{2+} signalling might be one aspect of the pathology in this disease. A connection between Ca^{2+}signalling and microdetachment might be, however, possible but has not been explored so far.

ACKNOWLEDGMENTS

We thank Gabi Fels (Charité, Berlin Germany) for technical support and Rita Rosenthal (Charité, Berlin Germany) for access to the confocal microscope. Open access funding enabled and organized by Projekt DEAL.

CONFLICT OF INTEREST

The authors declare that there is no conflict of interest associated with this manuscript.

AUTHOR CONTRIBUTIONS

N. Reichhart and O. Strauß are equal last authors of this work. Experiments were designed by N. Reichhart and O. Strauß and performed by M. Cordes, P. Bucichowski, and N. Reichhart. Data analysis was carried out by A.S. Alfaar, M. Cordes, and N. Reichhart. S.H. Tsang isolated, generated, and provided iPS cells from Best patient. S. Almedawar generated, and provided iPS cells from WT donors and differentiated them into RPE cells. S. Almedawar differentiated IPS cells obtained by S.H. Tsang into RPE cells. Manuscript was written by N. Reichhart and O. Strauß and revised by all authors.

REFERENCES

1. Marquardt A, Stohr H, Passmore LA, Kramer F, Rivera A, Weber BH. Mutations in a novel gene, VMD2, encoding a protein of unknown properties cause juvenile-onset vitelliform macular dystrophy (Best's disease). *Hum Mol Genet*. 1998;7:1517-1525.
2. Petrukhin K, Koisti MJ, Bakall B, et al. Identification of the gene responsible for Best macular dystrophy. *Nat Genet*. 1998;19:241-247.
3. Boon CJ, Klevering BJ, Leroy BP, Hoyng CB, Keunen JE, den Hollander AI. The spectrum of ocular phenotypes caused by mutations in the BEST1 gene. *Prog Retin Eye Res*. 2009;28:187-205.
4. Hartzell HC, Qu Z, Yu K, Xiao Q, Chien LT. Molecular physiology of bestrophins: multifunctional membrane proteins linked to best disease and other retinopathies. *Physiol Rev*. 2008;88:639-672.
5. Johnson AA, Guziewicz KE, Lee CJ, et al. Bestrophin 1 and retinal disease. *Prog Retin Eye Res*. 2017;58:45-69.
6. Marmorstein AD, Marmorstein LY, Rayborn M, Wang X, Hollyfield JG, Petrukhin K. Bestrophin, the product of the Best vitelliform macular dystrophy gene (VMD2), localizes to the basolateral plasma membrane of the retinal pigment epithelium. *Proc Natl Acad Sci USA*. 2000;97:12758-12763.
7. Strauss O. The retinal pigment epithelium in visual function. *Physiol Rev*. 2005;85:845-881.
8. Guziewicz KE, Sinha D, Gomez NM, et al. Bestrophinopathy: an RPE-photoreceptor interface disease. *Prog Retin Eye Res*. 2017;58:70-88.
9. Arden GB, Constable PA. The electro-oculogram. *Prog Retin Eye Res*. 2006;25:207-248.
10. Bakall B, Radu RA, Stanton JB, et al. Enhanced accumulation of A2E in individuals homozygous or heterozygous for mutations in BEST1 (VMD2). *Exp Eye Res*. 2007;85:34-43.
11. Marmorstein AD, Kinnick TR. Focus on molecules: bestrophin (best-1). *Exp Eye Res*. 2007;85:423-424.
12. Tsunenari T, Nathans J, Yau KW. Ca^{2+}-activated Cl^- current from human bestrophin-4 in excised membrane patches. *J Gen Physiol*. 2006;127:749-754.
13. Milenkovic VM, Rohrl E, Weber BH, Strauss O. Disease-associated missense mutations in bestrophin-1 affect cellular trafficking and anion conductance. *J Cell Sci*. 2011;124:2988-2996.
14. Johnson AA, Lee YS, Stanton JB, et al. Differential effects of Best disease causing missense mutations on bestrophin-1 trafficking. *Hum Mol Genet*. 2013;22:4688-4697.
15. Milenkovic A, Milenkovic VM, Wetzel CH, Weber BHF. BEST1 protein stability and degradation pathways differ between autosomal dominant Best disease and autosomal recessive bestrophinopathy accounting for the distinct retinal phenotypes. *Hum Mol Genet*. 2018;27:1630-1641.
16. Milenkovic A, Schmied D, Tanimoto N, Seeliger MW, Sparrow JR, Weber BHF. The Y227N mutation affects bestrophin-1 protein stability and impairs sperm function in a mouse model of Best vitelliform macular dystrophy. *Biol Open*. 2019;8:bio041335.
17. Mullins RF, Oh KT, Heffron E, Hageman GS, Stone EM. Late development of vitelliform lesions and flecks in a patient with best disease: clinicopathologic correlation. *Arch Ophthalmol*. 2005;123:1588-1594.
18. Guziewicz KE, Cideciyan AV, Beltran WA, et al. BEST1 gene therapy corrects a diffuse retina-wide microdetachment modulated by light exposure. *Proc Natl Acad Sci USA*. 2018;115:E2839-E2848.
19. Marmorstein AD, Johnson AA, Bachman LA, et al. Mutant Best1 expression and impaired phagocytosis in an iPSC model of autosomal recessive bestrophinopathy. *Sci Rep*. 2018;8:4487.
20. Singh R, Kuai D, Guziewicz KE, et al. Pharmacological modulation of photoreceptor outer segment degradation in a human iPS cell model of inherited macular degeneration. *Mol Ther*. 2015;23:1700-1711.
21. Singh R, Shen W, Kuai D, et al. iPS cell modeling of Best disease: insights into the pathophysiology of an inherited macular degeneration. *Hum Mol Genet*. 2013;22:593-607.
22. Milenkovic A, Brandl C, Milenkovic VM, et al. Bestrophin 1 is indispensable for volume regulation in human retinal pigment epithelium cells. *Proc Natl Acad Sci USA*. 2015;112:E2630-2639.
23. Guziewicz KE, McTish E, Dufour VL, et al. Underdeveloped RPE apical domain underlies lesion formation in canine bestrophinopathies. *Adv Exp Med Biol*. 2018;1074:309-315.
24. Yu K, Xiao Q, Cui G, Lee A, Hartzell HC. The best disease-linked Cl^- channel hBest1 regulates Ca V 1 (L-type) Ca^{2+} channels via src-homology-binding domains. *J Neurosci*. 2008;28:5660-5670.
25. Milenkovic VM, Krejcova S, Reichhart N, Wagner A, Strauss O. Interaction of bestrophin-1 and Ca^{2+} channel beta-subunits: identification of new binding domains on the bestrophin-1 C-terminus. *PLoS One*. 2011;6:e19364.
26. Reichhart N, Milenkovic VM, Halsband CA, Cordeiro S, Strauss O. Effect of bestrophin-1 on L-type Ca^{2+} channel activity depends on the Ca^{2+} channel beta-subunit. *Exp Eye Res*. 2010;91:630-639.
27. Barro-Soria R, Aldehni F, Almaca J, Witzgall R, Schreiber R, Kunzelmann K. ER-localized bestrophin 1 activates Ca^{2+}-dependent ion channels TMEM16A and SK4 possibly by acting as a counterion channel. *Pflugers Arch*. 2010;459:485-497.
28. Gomez NM, Tamm ER, Straubeta O. Role of bestrophin-1 in store-operated calcium entry in retinal pigment epithelium. *Pflugers Arch*. 2013;465:481-495.
29. Marmorstein LY, Wu J, McLaughlin P, et al. The light peak of the electroretinogram is dependent on voltage-gated calcium channels and antagonized by bestrophin (best-1). *J Gen Physiol*. 2006;127:577-589.
30. Neussert R, Muller C, Milenkovic VM, Strauss O. The presence of bestrophin-1 modulates the Ca^{2+} recruitment from Ca^{2+} stores in the ER. *Pflugers Arch*. 2010;460:163-175.
31. Strauss O, Muller C, Reichhart N, Tamm ER, Gomez NM. The role of bestrophin-1 in intracellular Ca(2+) signaling. *Adv Exp Med Biol*. 2014;801:113-119.

32. Zhang YW, Stanton JB, Wu J, et al. Suppression of Ca^{2+} signaling in a mouse model of Best disease. *Hum Mol Genet*. 2010;19:1108-1118.
33. Rosenthal R, Bakall B, Kinnick T, et al. Expression of bestrophin-1, the product of the VMD2 gene, modulates voltage-dependent Ca^{2+} channels in retinal pigment epithelial cells. *FASEB J*. 2006;20:178-180.
34. Strauss O, Reichhart N, Gomez NM, Muller C. Contribution of Ion channels in calcium signaling regulating phagocytosis: MaxiK, Cav1.3 and Bestrophin-1. *Adv Exp Med Biol*. 2016;854:739-744.
35. Wu J, Marmorstein AD, Striessnig J, Peachey NS. Voltage-dependent calcium channel CaV1.3 subunits regulate the light peak of the electroretinogram. *J Neurophysiol*. 2007;97:3731-3735.
36. Constable PA. Nifedipine alters the light-rise of the electro-oculogram in man. *Graefe's Arch Clin Exp Ophthalmol*. 2011;249(5):677–684. https://doi.org/10.1007/s00417-010-1604-6.
37. Muller C, Mas Gomez N, Ruth P, Strauss O. CaV1.3 L-type channels, maxiK Ca(2+)-dependent K(+) channels and bestrophin-1 regulate rhythmic photoreceptor outer segment phagocytosis by retinal pigment epithelial cells. *Cell Signal*. 2014;26:968-978.
38. Zhu Y, Carido M, Meinhardt A, et al. Three-dimensional neuroepithelial culture from human embryonic stem cells and its use for quantitative conversion to retinal pigment epithelium. *PLoS One*. 2013;8(1):e54552.
39. Rosenthal R, Thieme H, Strauss O. Fibroblast growth factor receptor 2 (FGFR2) in brain neurons and retinal pigment epithelial cells act via stimulation of neuroendocrine L-type channels (Ca(v)1.3). *FASEB J*. 2001;15:970-977.
40. Miller SS, Edelman JL. Active ion transport pathways in the bovine retinal pigment epithelium. *J Physiol*. 1990;424:283-300.
41. Tsunenari T, Sun H, Williams J, et al. Structure-function analysis of the bestrophin family of anion channels. *J Biol Chem*. 2003;278:41114-41125.
42. Marmorstein AD, Kinnick TR, Stanton JB, Johnson AA, Lynch RM, Marmorstein LY. Bestrophin-1 influences transepithelial electrical properties and Ca^{2+} signaling in human retinal pigment epithelium. *Mol Vis*. 2015;21:347-359.
43. Yang T, Liu Q, Kloss B, et al. Structure and selectivity in bestrophin ion channels. *Science*. 2014;346:355-359.
44. Keckeis S, Reichhart N, Roubeix C, Strauss O. Anoctamin2 (TMEM16B) forms the Ca(2+)-activated Cl(-) channel in the retinal pigment epithelium. *Exp Eye Res*. 2017;154:139-150.
45. Park M, Jung HG, Kweon HJ, Kim YE, Park JY, Hwang EM. The E3 ubiquitin ligase, NEDD4L (NEDD4-2) regulates bestrophin-1 (BEST1) by ubiquitin-dependent proteolysis. *Biochem Biophys Res Commun*. 2019;514:344-350.
46. Marmorstein LY, McLaughlin PJ, Stanton JB, Yan L, Crabb JW, Marmorstein AD. Bestrophin interacts physically and functionally with protein phosphatase 2A. *J Bio Chem*. 2002;277:30591-30597.
47. Karl MO, Kroeger W, Wimmers S, et al. Endogenous Gas6 and Ca^{2+}-channel activation modulate phagocytosis by retinal pigment epithelium. *Cell Signal*. 2008;20:1159-1168.
48. Korkka I, Viheriala T, Juuti-Uusitalo K, et al. Functional voltage-gated calcium channels are present in human embryonic stem cell-derived retinal pigment epithelium. *Stem Cells Transl Med*. 2019;8:179-193.

SUPPORTING INFORMATION

Additional supporting information may be found online in the Supporting Information section.

How to cite this article: Cordes M, Bucichowski P, Alfaar AS, et al. Inhibition of Ca^{2+} channel surface expression by mutant bestrophin-1 in RPE cells. *The FASEB Journal*. 2020;34:4055–4071. https://doi.org/10.1096/fj.201901202RR